J. Fluid Mech. (1975), *vol.* 72, *part* 4, *pp.* 731–751
Printed in Great Britain

An experimental investigation of the stability of plane Poiseuille flow

By M. NISHIOKA, S. IIDA AND Y. ICHIKAWA
College of Engineering, University of Osaka Prefecture, Japan

(Received 5 May 1975)

Stability experiments were made on plane Poiseuille flow generated in a long channel of a rectangular cross-section with a width-to-depth ratio of 27·4. By reducing the background turbulence down to a level of 0·05 %, we succeeded in maintaining the flow laminar at Reynolds numbers up to 8000, which is much larger than the critical Reynolds number of the linear theory, about 6000. The downstream development of the sinusoidal disturbance introduced by the vibrating ribbon technique was studied in detail at various frequencies in the range of Reynolds number from 3000 to 7500. This paper presents the experimental results and clarifies the linear stability, the nonlinear subcritical instability and the breakdown leading to the transition.

1. Introduction

The behaviour of a sinusoidal disturbance of finite amplitude in plane Poiseuille flow has been a principal subject of many theoretical studies on hydrodynamic stability. Stuart (1971) reviewed earlier theoretical work on this topic. To the present authors, the most interesting of the theoretical results is the prediction that subcritical instability occurs in a plane Poiseuille flow (i.e. disturbances can grow below the critical Reynolds number of the linear theory, provided their amplitude lies above some threshold value). According to Lin (1955), Thomas (1953) and Ito (1974*a*), the critical Reynolds number, based on the half-depth of the channel and the centre-plane velocity, is about 6000. The prediction was made first by Meksyn & Stuart (1951) and later confirmed by Reynolds & Potter (1967) and Pekeris & Shkoller (1967), through calculations based on the nonlinear theory of Stuart (1960) and Watson (1960). Recently, Ito (1974*b*) solved the nonlinear equation for spatially growing disturbances by modifying the method of Watson (1962). Giving the solutions for wider ranges of the Reynolds number and the frequency of disturbance, Ito (1974*b*) also showed that subcritical instability exists.

On the laminar instability, numerous experiments have been made for various kinds of flow, since Schubauer & Skramstad (1943) first verified the linear theory for Blasius flow, but there are not many experiments for flows in rectangular channels. To the authors' knowledge, the only one is that of Kao & Park (1970). Using artificial excitation, they examined behaviour of sinusoidal disturbances in a channel with an aspect ratio (width-to-depth ratio of channel) of 8, to determine the neutral-stability curve. But, because the aspect ratio was not very

large, the result did not agree with that of the linear theory for plane Poiseuille flow. For example, the critical Reynolds number was about 1100, being much smaller than the theoretical value of about 6000. Transition to turbulence in rectangular channels was investigated by Davies & White (1928), Badri Narayanan & Narayana (1967), Patel & Head (1969) and others. In these experiments, the transition occurred at Reynolds numbers less than 2500, with abrupt appearance of turbulent bursts. Using a channel with an aspect ratio of 70, Karnitz, Potter & Smith (1974) succeeded in maintaining the flow laminar up to a Reynolds number of 5000, by reducing the background turbulence down to a level of 0·3 %. They found that sinusoidal disturbances preceded turbulent bursts, but they did not examine the sinusoidal disturbance in detail. Thus, to date, the theoretical results for the linear and nonlinear stabilities of plane Poiseuille flow have not been conclusively verified by experiment.

In the experiments described in the present paper, we used a channel with an aspect ratio of 27·4. By reducing the background turbulence down to a level of 0·05 %, we succeeded in maintaining the flow laminar at Reynolds numbers up to 8000. The downstream development of the sinusoidal disturbance, introduced by means of a vibrating ribbon, was examined in detail at various frequencies in the range of Reynolds number from 3000 to 7500. This paper includes experimental results on the linear stability, the nonlinear subcritical instability and the breakdown leading to the transition.

2. Experimental apparatus and preliminary tests

2.1. *Wind tunnel*

The experiments were conducted in a rectangular channel, whose width, depth and length were respectively 40, 1·46 and 600 cm, as shown in figure 1. The aspect ratio is 27·4. The half-depth h, on which the Reynolds number R is defined, is 0·73 cm. The channel is made of smooth Plexiglas (1 cm thick). Metal frames keep the channel free from warping. The flow is generated by a Sirocco fan at the upstream end of the tunnel, and discharged into the atmosphere at the downstream end of the channel. The velocity on the channel centre-plane U_c could be varied from 0 to 25 m s^{-1} by throttling a valve at the entrance of the fan. Five damping screens (100 mesh) span the diffuser and the settling chamber. The contraction is two-dimensional, with contraction ratio 27·4. This arrangement reduced the background turbulence to a level of 0·05 % at $U_c = 12$ m s^{-1}. The level is almost independent of U_c, so long as the flow remains laminar. The wave form of the background turbulence is almost sinusoidal, because a significant contribution (not less than 80 %) comes from sinusoidal fan noise of 715 Hz. Under the present experimental conditions, the frequency 715 Hz is one order of magnitude higher than the frequencies of unstable disturbances predicted by the linear theory. Thus, we may consider that the background turbulence is essentially less than 0·01 %.

The x, y, z co-ordinate system adopted is shown also in figure 1. The x axis is measured from the entrance of the channel in the streamwise direction; the y axis is normal to the lower and upper walls, being measured from the centre-plane;

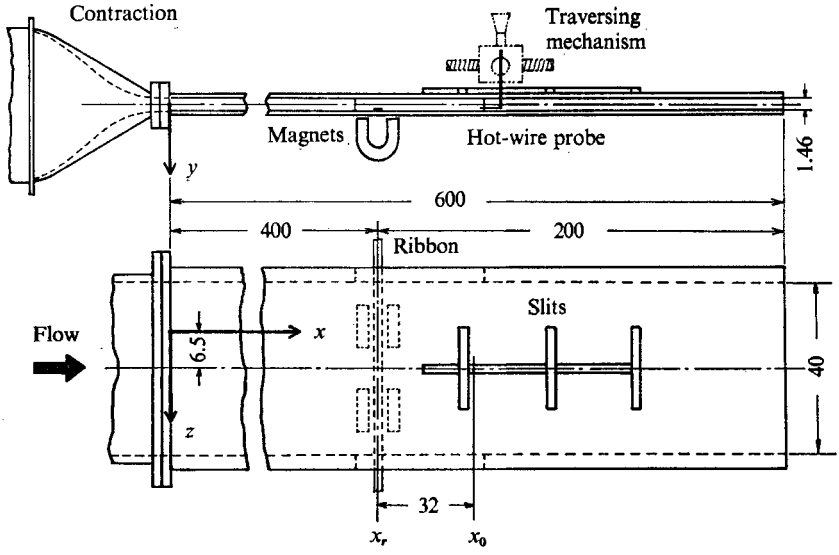

Figure 1. Channel apparatus and co-ordinate system. Dimensions in centimetres.

and the z axis is in the spanwise direction, its origin displaced from the spanwise centre by 6·5 cm. In this co-ordinate system the lower wall is at $y/h = 1{\cdot}0$. The upper wall contains slits (1·2 cm wide) in the test section in the x and z directions; a hot-wire probe mounted on a two-dimensional traversing mechanism is inserted into the test section through one of these. The slits were covered to prevent air leakage. Those not in use were filled up perfectly; that in use was covered with a block, which contained its own slit (about 0·3 cm wide) and sliding plate. It was inevitable that the upper wall should exhibit warping around the slits owing to the machining. The extent of this was examined along the spanwise and streamwise slits, and it was found that the magnitude of the depth variation due to warping was at most 1·5 % of the mean depth (1·46 cm) in both directions. An effect of that variation on the basic flow will be mentioned later. Pressure holes of 0·5 mm diameter were drilled on the lower wall along a line $z = 16{\cdot}5$ cm, at an interval of 10 cm, for wall-pressure measurements.

2.2. *Hot-wire anemometer*

Velocity measurements were made by a low-noise, constant-temperature hot-wire anemometer, with a linearizer (Nishioka & Sato 1970). The frequency response of the hot-wire system was flat up to 10 kHz. The hot wire was copper-plated tungsten, 3·8 μm in diameter, with 2·5 mm sensitive length. Diameters of the hot-wire supports, made of steel, were 0·5 mm at the roots, and 0·1 mm at tips to which the hot wire was welded. The probe stem, made of stainless steel 3 mm in diameter, generated a turbulent wake; therefore the whole channel flow became turbulent some distance downstream from the stem. It was plausible to conjecture that the turbulence wedge had some upstream influence. To keep the flow around the hot wire free from such effects, the distance of the hot wire from the stem (i.e. the length of the supports) was made comparable to the

wavelength of the disturbance to be investigated, which was about 5 cm. The hot wire was always oriented so as to pick up the x component. The calibration made before and after each test run was reproducible to within 3 %.

2.3. *Transition Reynolds number*

In the present experiments, the transition to turbulence never took place at $R < 8000$ without artificial excitations; and it was sometimes possible to maintain the flow laminar up to $R = 9000$. This is attributed to the fact that the background turbulence was quite low, being about 0·05 %. As described later, the stability experiments show that the critical Reynolds number for the linear instability is about 6000, and the spatial growth rate of unstable disturbances is quite small, so long as their amplitude remains small. In other words, at $R < 8000$ or 9000, small disturbances need a distance larger than the length of the present channel to grow in amplitude to the degree sufficient for triggering the transition.

The natural transition is preceded by intermittent bursts of irregular velocity fluctuations, similar to those of the turbulent spot found in the transition process of Blasius flow. As a prelude to each burst, there appear sinusoidal velocity fluctuations, with frequencies just outside the upper branch of the neutral curve of the linear theory. The spot-like fluctuations were not examined in detail.

2.4. *Measurements of basic flow*

To ascertain the flow in the test section to be regarded as a plane Poiseuille flow, the velocity distribution and the streamwise variation of wall pressure were examined in detail at $R = 3000$–7500. The pressure measurements show that the streamwise pressure gradient decreases rapidly immediately downstream from the channel entrance, but it soon approaches a constant value (e.g. the gradient is maintained constant at $x > 200$ cm at $R = 7500$). The constant gradients at various Reynolds numbers agree with the theoretical value for plane Poiseuille flow.

The spanwise distributions of the centre-plane velocity U_c are given in figure 2, to show the degree of the two-dimensionality at $x = 425$ cm, at various Reynolds numbers. R is calculated with the value of U_c at $z = 6{\cdot}5$ cm (i.e. at the position of the streamwise slit indicated by an arrow in the figure). The distributions are flat at $R \leqslant 3500$, but wavy at $R > 3500$. As R increases, the wavy distortion grows without essentially changing the pattern. The pattern closely resembles that of the slight warping of the upper wall, mentioned before. For this reason, it is thought that the slight three-dimensionality at $R > 3500$ is caused by the depth variation in the spanwise direction. The wavy distortion disappears when the flow becomes fully turbulent, as the figure shows. It is said that the appearance of the wavy distortion is peculiar to the laminar flow. At $R \leqslant 3500$, the velocity distribution across the depth agrees almost completely with the theoretical parabolic distribution at any spanwise position. As R increases, the distribution undergoes distortion and becomes asymmetric. The most asymmetric distributions are those measured at $z = 3$ and 6 cm at $R = 7500$; and in figure 3 they are compared with the parabolic distribution, together with

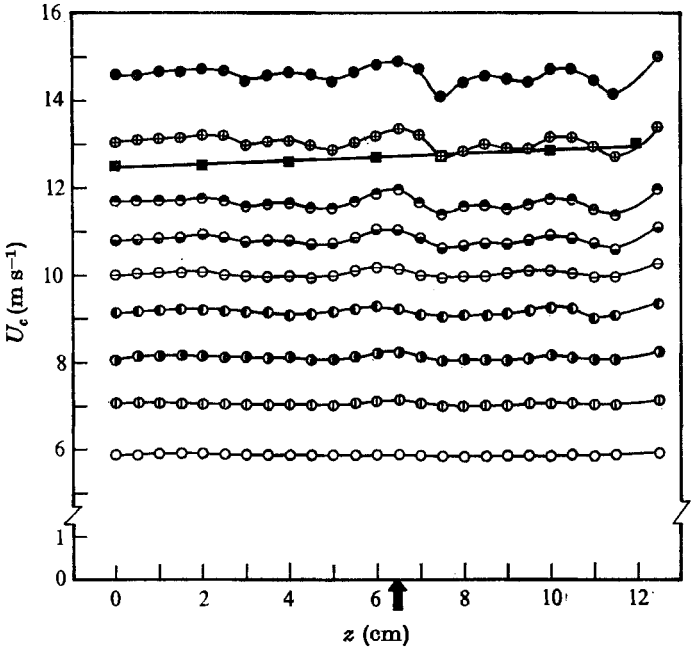

FIGURE 2. Spanwise distributions of velocity on the centre-plane U_c. Arrow indicates position of the streamwise slit, $z = 6{\cdot}5$ cm. ■, fully developed turbulent flow. Fully developed laminar flow:

R ($\times 10^{-2}$)	30	35	40	45	50	55	59	65	73
	○	⊙	◑	◐	⊖	◒	◓	⊕	●

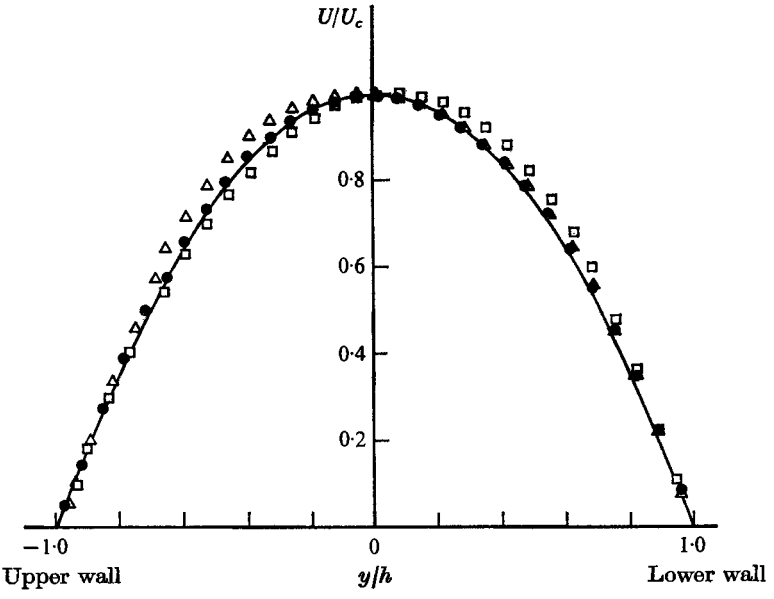

FIGURE 3. Velocity distributions across the depth at various spanwise positions. $R = 7500$. —, parabolic distribution.

z (cm)	3·0	6·0	9·0
	□	△	●

a symmetric distribution at $z = 9$ cm. Figures 2 and 3 show that the distortion of the two-dimensionality, and the deviation from the parabolic distribution never exceed 6 %, even in the worst case, i.e. $R = 7500$.

2.5. *Procedure of stability experiments*

A sinusoidal disturbance was introduced into the basic flow by the so-called vibrating ribbon technique (Schubauer & Skramstad 1943). As shown in figure 1, a phosphor bronze ribbon (0·05 mm thick, 4 mm wide and 80 cm long) was stretched close to the lower wall, under tension by means of weights. The segment inside the channel, 40 cm long, was free to vibrate normal to the wall, when driven by a sinusoidal electric current in a steady magnetic field produced by permanent magnets attached to the opposite side of the wall. The exciting current was supplied by a sine-wave generator through a power amplifier; and the frequency could be varied in a desired range.

It was shown, from preliminary observations of small disturbances, that some distance from the ribbon was required for the disturbances to establish a structure which did not change downstream. Therefore the ribbon was located at the upstream end of the test section; the position of the ribbon $x_r = 400$ cm. The magnitude of disturbance was controlled by varying either the magnitude of the exciting current, or the height of the ribbon from the wall. The experiments on small disturbances were made at heights of 0·15, 0·3 and 0·85 mm; those on large disturbances were made at a height of 0·85 mm. At heights beyond 1 mm, a flutter occurs often, and a precise experiment is difficult. The ribbon has no undesirable effect on the flow at the heights adopted.

Wave forms of x-component fluctuations (u fluctuations) were observed with a cathode-ray oscilloscope. The root-mean-square value $u' \equiv (\overline{u^2})^{\frac{1}{2}}$ was measured with an r.m.s. voltmeter. Phase angles of u fluctuations were measured with the oscilloscope, using the input to the ribbon as a phase reference. Spectral analyses of u fluctuations were made with a RC band-pass filter, whose bandwidth was 3 % of the centre frequency at 3 dB attenuation.

3. Results and discussion

3.1. *Nature of small disturbances*

The linear stability theory shows that the antisymmetric u fluctuation, with respect to the centre-plane, gives a lower critical Reynolds number than the symmetric one. So it was intended to generate the antisymmetric disturbance in the present experiments. The variations in y of the amplitude and phase of u fluctuations are illustrated in figure 4 (plate 1), which shows oscilloscope traces of a disturbance with $f = 82$ Hz at $R = 6000$. The photographs were taken at $x - x_r = 32$ cm; the upper trace in each photograph is the u fluctuation, the lower the exciting current. As photograph (*a*) shows, the primary fluctuation is purely sinusoidal, though it is accompanied by a weak fluctuation of 715 Hz (the fan noise). In photographs (*b*)–(*g*) the noise was diminished, using the band-pass filter. The amplitude became nearly zero at $y = 0$, where a sharp 180° phase shift occurred. (See photographs (*c*)–(*g*).) Photographs (*e*)–(*g*) indicate that a small

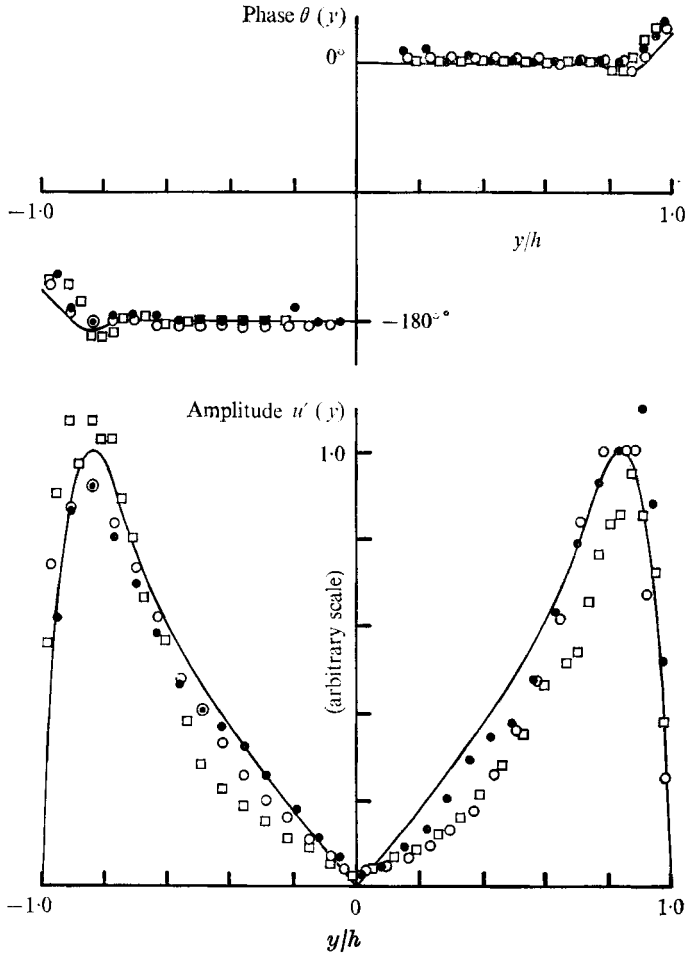

FIGURE 5. Amplitude and phase distributions of small disturbances. ——, Ito's theoretical result for β ($\equiv 2\pi fh/U_c$) = 0·27 at R = 4000. Our experimental conditions were as follows:

R ($\times 10^{-2}$)	30	40	60
f (Hz)	47·0	50·4	82·0
β	0·36	0·27	0·32
	○	●	□

phase shift occurred also near the wall. These features are more properly illustrated in figure 5, which shows the amplitude and phase distributions for disturbances at (R,f) = (3000, 47), (4000, 50·4) and (6000, 82 Hz), all measured at $x-x_r$ = 25 cm. As the amplitude, the r.m.s. value u' is plotted on an arbitrary scale. Each amplitude distribution is symmetric with respect to the centre-plane, having two maxima near $y/h = \pm 0{\cdot}85$; the maximum value U'_m is less than $0{\cdot}01U_c$. The phase difference at any points symmetrical with respect to the centre-plane is always 180°, in each case. Thus, the sinusoidal disturbance is antisymmetric.

A large number of similar measurements were made along the streamwise slit at $x-x_r \geqslant 32$ cm, with various values of R and f. Measurements of streamwise

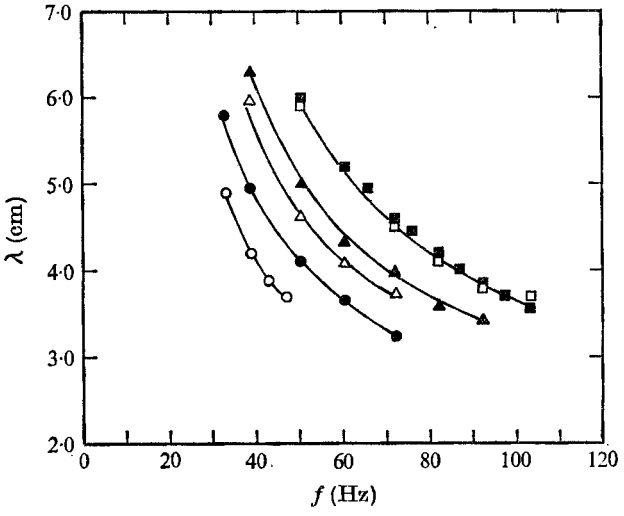

FIGURE 6. Wavelengths of small disturbances.

R ($\times 10^{-2}$)	30	40	50	60	70	75
	○	●	△	▲	□	■

phase variation show that the disturbance is indeed a travelling wave. It appears that whether a disturbance damps or grows while travelling downstream is strongly dependent on its initial magnitude. In fact, it is found that even a disturbance which damps according to the linear theory when its amplitude is small does grow downstream when its amplitude exceeds a certain threshold. We focus our attention first on disturbances of small amplitude.

3.1.1. *Linear development.* For a small disturbance, it is found that damping and amplification depend merely on R and f, and that the structure does not change much downstream. Phase distribution is independent of amplitude, and wavelength is independent of distance from the ribbon. The measured wavelength λ is plotted against f in figure 6 at various Reynolds numbers. The phase velocity C given from the relation $C = f\lambda$ varies from $0{\cdot}2U_c$ to $0{\cdot}3U_c$ for the ranges of R and f examined. The behaviour of the small disturbance may be called linear development.

To illustrate the linear development more clearly, the non-dimensional maximum value $u'_m/u'_{m,0}$ is plotted on a logarithmic scale against $x-x_0$ in figures 7(*a*) and (*b*), where $x_0 - x_r = 32$ cm and $u'_{m,0} = u'_m(x_0)$. Figure 7(*a*) shows the results for a fixed frequency $f = 72$ Hz at various Reynolds numbers and illustrates the effect of the Reynolds number: damped at $R = 4000$ and 5300, nearly neutral at $R = 6400$, and amplified at $R = 7000$. On the other hand, figure 7(*b*) shows the results at a fixed Reynolds number $R = 7000$ at various frequencies: amplified at $f = 60$ and 72 Hz, nearly neutral at $f = 50$ Hz, and damped at $f = 82$ and 92 Hz. From these figures we may conclude that a small disturbance damps or grows exponentially in the streamwise direction.

3.1.2. *Two-dimensionality of the small disturbance.* The amplitude and phase distributions of a disturbance with $f = 82$ Hz measured at various spanwise

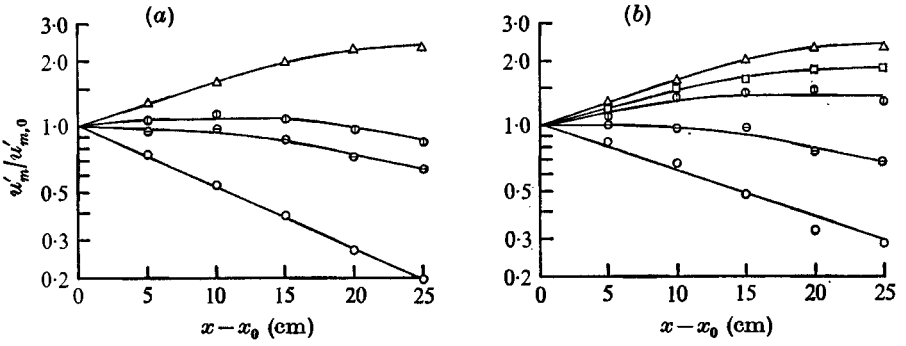

FIGURE 7. Linear development of small disturbances: streamwise growth of decay of non-dimensional maximum in fluctuation $u'_m/u'_{m,0}$. Results for fixed (*a*) frequency $f = 72$ Hz, (*b*) Reynolds number $R = 7000$.

(*a*)	R ($\times 10^{-2}$)	40	53	64	70	
		○	⊖	⊕	△	
(*b*)	f (Hz)	50	60	72	82	92
		⊕	□	△	⊖	○

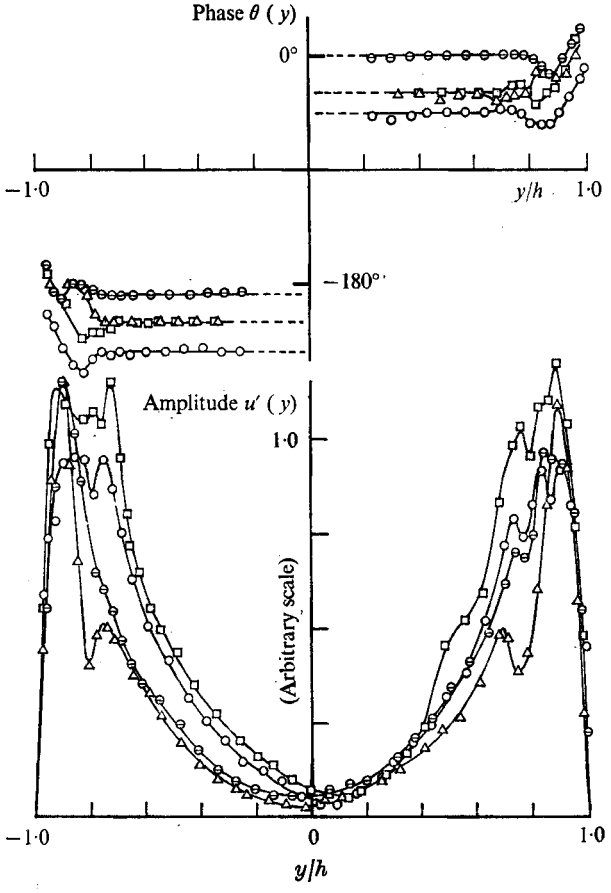

FIGURE 8. Examination of two-dimensionality of small disturbances. Amplitude and phase distributions at various spanwise positions at $R = 7500$ and $f = 82$ Hz.

z (cm)	0	3·0	6·0	9·0
	⊖	□	△	○

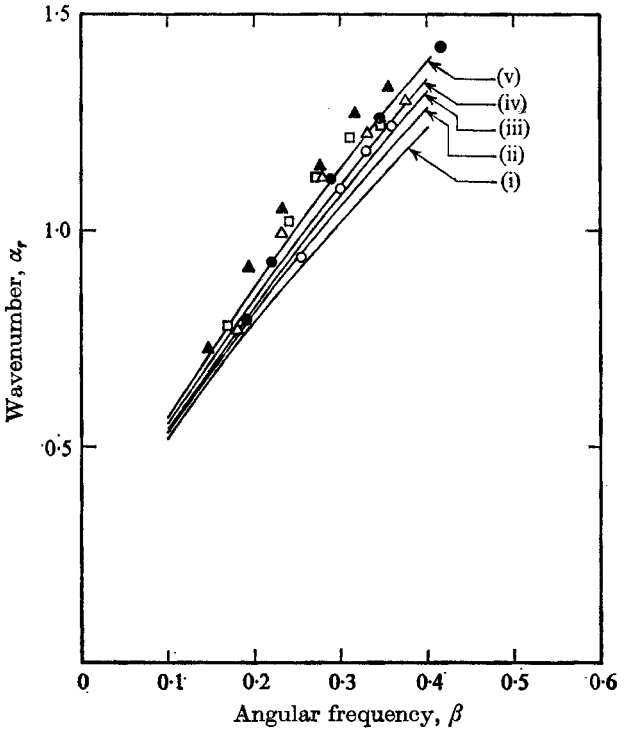

FIGURE 9. Wavenumber α_r against angular frequency β.

	R ($\times 10^{-2}$)				
	30	40	50	60	80
Theory (Ito)	(i)	(ii)	(iii)	(iv)	(v)
	30	40	50	60	70
Present	○	●	△	▲	□

positions at $R = 7500$ are given in figure 8, to show the degree of the two-dimensionality. The amplitude is plotted on an arbitrary scale, but the relative magnitudes are expressed correctly. The amplitude distributions at different spanwise positions differ in magnitude, but their shapes are similar, except for small dips at $0{\cdot}7 < |y/h| < 0{\cdot}9$. The phase angle is plotted in such a way that its shift in the spanwise direction can be observed. The phase distributions have almost the same shape, except for small distortions at $z = 0$ and 6 cm, corresponding to the dips in the amplitude distributions at the same positions. The shifts in the spanwise direction are nearly independent of y, and the amount of the shift between $z = 0$ and 9 cm is less than 50°. This is quite small, considering that the wavelength of the disturbance is 4·2 cm. Thus, the disturbance is approximately two-dimensional.

3.1.3. *Comparison with the linear stability theory.* The structure and the behaviour of the small disturbances may be well described by the expression adopted in the linear stability theory:

$$u = \mathrm{Re}\{\sqrt{2}u'(y)\exp[i(\alpha x - \beta t - \theta(y))]\}.$$

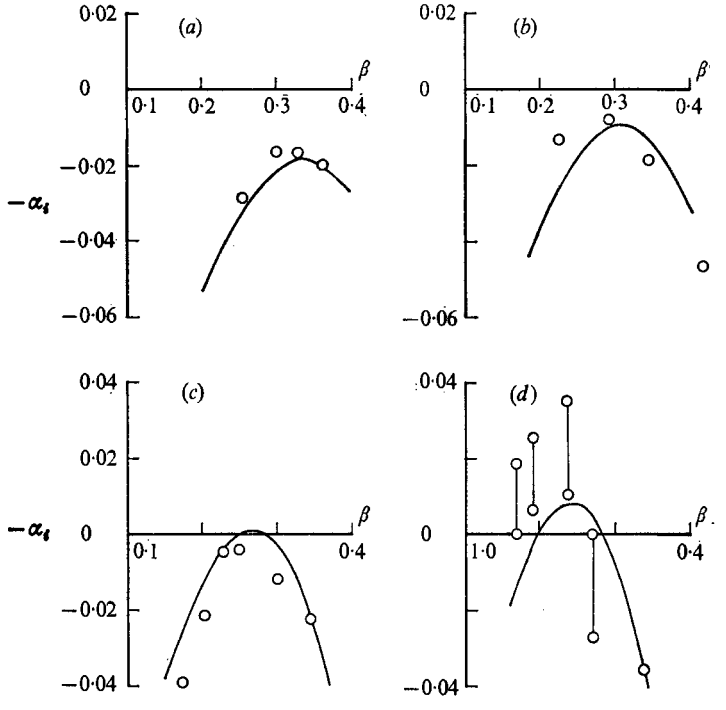

FIGURE 10. Amplification rate $-\alpha_i$ against angular frequency β.

		R ($\times 10^{-2}$)			
		(*a*)	(*b*)	(*c*)	(*d*)
Theory (Ito)	——	30	40	60	80
Present	○	30	40	57	70

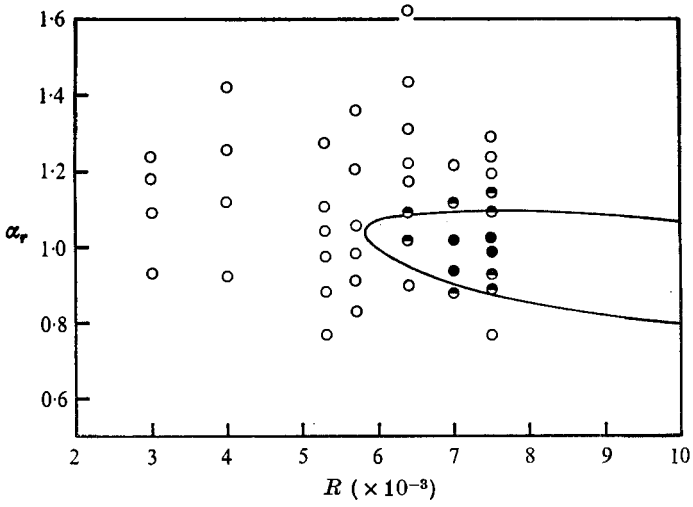

FIGURE 11. Stability boundary for small disturbances. ——, Ito's neutral curve. Our results: ○, damped; ◓, nearly neutral; ●, amplified.

$\sqrt{2}u'(y)$ and $\theta(y)$ are real quantities, representing amplitude and phase distributions, respectively. The angular frequency β is also real, but α is complex. Its real part α_r denotes the wavenumber; and the imaginary part α_i, the spatial damping rate (or $-\alpha_i$ the amplification rate). We now describe our experimental results in terms of α and β (which are made non-dimensional by using h and U_c as the scales). At the same time, we compare them with those of the linear stability calculation carried out by Ito (1974*a*). The comparisons of $u'(y)$ and $\theta(y)$ have been made in figure 5. It is here noted that the amplitude and phase distributions do not depend on R and f strongly, as shown in figure 5. Figure 9 shows the relation between

$$\alpha_r \equiv 2\pi h/\lambda \quad \text{and} \quad \beta \equiv 2\pi f h/U_c.$$

Experimentally, the amplification rate is determined from

$$-\alpha_i = h\, d \ln u'_m/dx.$$

The value thus obtained is plotted against β in figure 10, which shows that the amplification rate is at most about 0·02 at $R = 7000$. This is quite small, considering that free boundary layers, such as jets and wakes, have amplification rates of about 0·2. Comparison with the neutral-stability curve is made in figure 11. The experimental value of the critical Reynolds number is about 6000, in agreement with Ito's theoretical value, 5771.

All comparisons made above show good, or fair, agreement, and that the small disturbance develops as predicted by linear stability theory.

3.2. *Outline of the breakdown*

For a supercritical growing disturbance with $f = 72$ Hz at $R = 7000$ (whose linear development is illustrated in figure 7), it is found that downstream development begins to deviate from exponential growth at a station where u'_m reaches about $0{\cdot}025U_c$, and the disturbance grows catastrophically downstream. This is one of the characteristic features of the nonlinear development of large disturbances, and eventually leads to the breakdown of periodic motions. Experiments of Klebanoff, Tidstrom & Sargent (1962) on the instability of Blasius flow show that, in the process of the breakdown, an inflexional velocity distribution with intense shear (evidenced by 'spikes' in the wave form of the u fluctuation) appears instantaneously for each cycle of the fundamental oscillation. They also show that, subsequently, higher-frequency motions called 'hairpin eddies' are generated, owing to a local secondary instability of the instantaneous velocity distribution. This happened in our experiments.

Oscilloscope traces, which illustrate the breakdown of a disturbance with $f = 72$ Hz and at $R = 7200$, are shown in figure 12 (plate 2). They were obtained for an arbitrary fixed ribbon current at various streamwise positions $x - x_0$ ($x_0 - x_r = 32$ cm) at $y/h = 0{\cdot}47$. The upper trace in each photograph is the u fluctuation (decreasing velocity is in a downward direction); values of u'/U_c and $x - x_0$ are noted in the caption. The lower trace is the input to the ribbon. The wave forms are purely sinusoidal at $x - x_0 = 12$ and 13 cm. At $x - x_0 = 14$ cm, a low-velocity pulse (a spike) begins to appear for each cycle, and grows

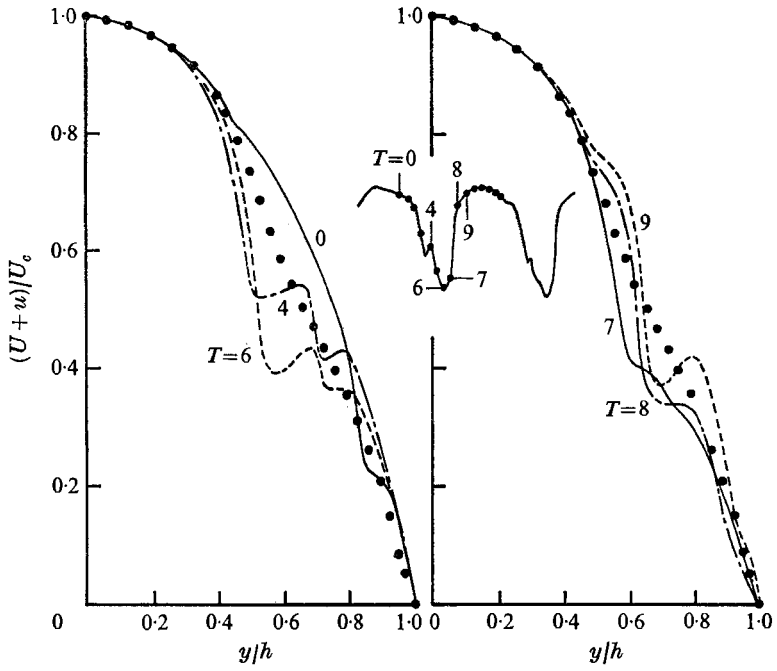

FIGURE 14. Instantaneous velocity distributions drawn from figures 13(*a*)–(*s*). Time T corresponding to each distribution is noted on the trace of the u fluctuation at $y/h = 0{\cdot}6$, sketched in the figure. ●, mean velocity.

catastrophically downstream. Suggesting formation of 'hairpin eddies'; higher-frequency oscillations appear at $x-x_0 = 16$ to 18 cm. The photographs show that the phase difference of the fundamental between $x-x_0 = 12$ and 18 cm is approximately 360° (i.e. the wavelength of the fundamental is about 6 cm there). Thus, the streamwise extent of the region where the whole process takes place, from appearance of spikes to formation of hairpin eddies, is smaller than one wavelength of the fundamental.

Wave forms of u fluctuations at various y positions at $x-x_0 = 15$ cm are shown in figure 13 (plate 3). The wave forms near the lower wall ($y/h = 1{\cdot}0$) are considerably distorted by the presence of higher harmonics of large amplitude. This feature is in contrast to the case of Blasius flow: Klebanoff *et al.* (1962, figure 26) showed that higher harmonics play no vital part at the initial stage of the breakdown. As for the fundamental, a sharp 180° phase shift occurs at $y = 0$, where the fluctuation becomes vanishingly small. No spikes appear at $y < 0$ (above the centre-plane), and there u fluctuations are much smaller than those at $y > 0$. This suggests that the breakdown is a local phenomenon, at least in its initial stage. The photographs show instantaneous velocity $(U+u)$. The fluctuations at various y positions are so regular that we can draw an instantaneous velocity distribution across the depth, at an arbitrary instant during the cycle, using the input to the ribbon (a purely sinusoidal wave in each photograph) as a time-marker. Figure 14 shows the instantaneous velocity distributions thus obtained for $y > 0$. The time T corresponding to each distribution is noted on the trace of the u fluctuation at $y/h = 0{\cdot}60$ sketched in the figure.

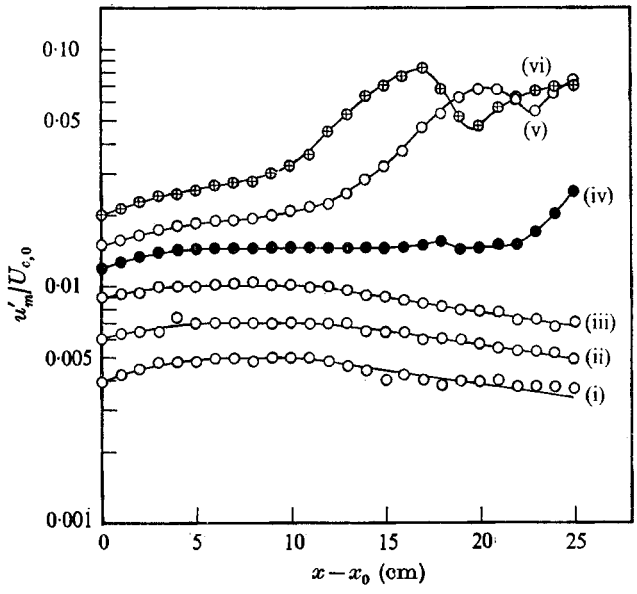

FIGURE 15. Growth or decay of a subcritical disturbance, with $f = 72$ Hz at $R = 5000$, depending on its initial intensity $u'_{m,0}/U_{c,0}$. Streamwise variations of maximum intensity u'_m/U shown at the following different values:

$u'_{m,0}/U_{c,0}$	0·004	0·006	0·009	0·012	0·015	0·020
	(i)	(ii)	(iii)	(iv)	(v)	(vi)

The mean velocity is represented by dots; U_c remains almost the same as the undisturbed value. Most instantaneous distributions are inflexional, having intense shear around $y/h = 0{\cdot}50$ at $T = 4$ to 6, and around $y/h = 0{\cdot}62$ at $T = 8$ to 9. Distributions at $T = 4$ to 6 are complicated with the presence of higher harmonics.

Klebanoff *et al.* (1962) showed that, as a prerequisite for the breakdown, streamwise vortices are generated owing to three-dimensional development of the fundamental with 'peak–valley' spanwise structure. At the present stage, we have not fully examined the three-dimensionality of large disturbances. But, especially at the later stage of the breakdown, various different features are observed at the same station, without apparent changes in the experimental conditions. This suggests that the flow is three-dimensional there.

In summary, it may be concluded that the breakdown occurs as a result of a local secondary instability of the inflexional velocity distribution, with intense shear appearing instantaneously for each cycle of the fundamental motion, just as happens in Blasius flow. The exponential growth of the small disturbance at $R > R_c$ always leads to the transition to turbulence through the breakdown. Thus, the so-called supercritical equilibrium flow was not realized in our experiments. (See Stuart 1971, for the equilibrium flow.)

3.3. *Nonlinear subcritical instability*

3.3.1. *Determination of the threshold value.* To find out how the downstream development of subcritical disturbances depends on their magnitude, the streamwise variation of the maximum r.m.s. value u'_m was examined, by changing the

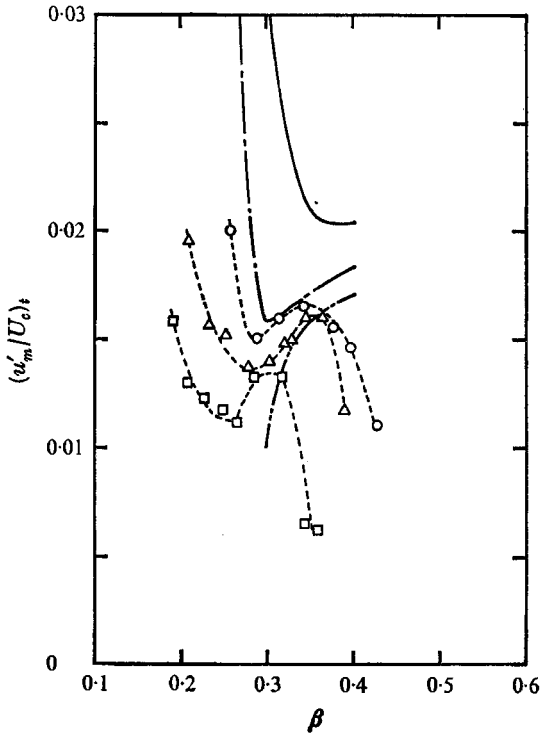

FIGURE 16. Threshold value for the subcritical instability $(u'_m/U_c)_t$ against angular frequency β.

R ($\times 10^{-2}$)	40	50	60
Theory (Ito)	——	— · —	— · · —
Present	○	△	□

initial intensity systematically. The results for a subcritical disturbance, with $f = 72$ Hz at $R = 5000$, are shown in figure 15. $u'_m/U_{c,0}$ is plotted on a logarithmic scale against $x - x_0$, where $x_0 - x_r = 32$ cm and $U_{c,0} = U_c(x_0)$. The intensity at $x = x_0$ (i.e. $u'_{m,0}/U_{c,0}$) is called the initial intensity. It was changed by varying the magnitude of the input to the ribbon. As the figure shows, at initial intensities less than 1 %, disturbances eventually damp downstream. This is the case of linear development. On the other hand, a disturbance with an initial intensity of 1·5 % grows downstream, gradually at first but rapidly later, and as a result the transition to turbulence occurs downstream. Increase in the initial intensity further beyond 1·5 % has no significant effects on the downstream development, except that the starting point of the rapid growth moves upstream. At an initial intensity of 1·2 %, the disturbance is nearly neutral over a considerable distance, though it is eventually amplified downstream. Figure 15 presents evidence for the theoretical prediction that subcritical instability occurs in a plane Poiseuille flow. The figure shows that the threshold value of u'_m/U_c for the instability is about 1·5 % in this example.

Similar observations were made at $R = 4000$, 5000 and 6000 at various frequencies, to examine the dependence of the threshold value on the Reynolds number and frequency. The results are given in figure 16, where the threshold

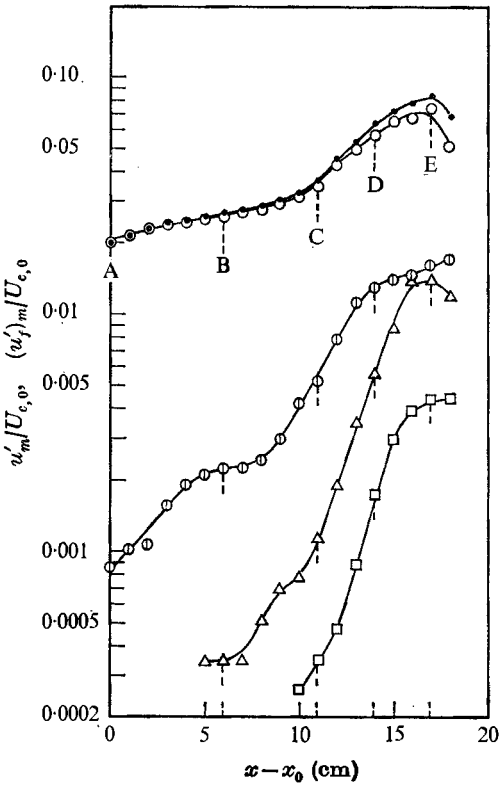

FIGURE 17. Streamwise variation of maximum intensities of total and harmonic components observed in the nonlinear subcritical growth of a disturbance with a fundamental frequency $f = 72$ Hz at $R = 5000$. ●, total; ○, fundamental (72 Hz); ⓘ, second (144); △, third (216); □, fourth (328). A–E, stations.

value $(u'_m/U_c)_t$ is plotted against $\beta\,(\equiv 2\pi fh/U_c)$. The figure includes theoretical results of Ito (1974*b*). Experimental curves at three different Reynolds numbers bear resemblance to each other; each has one minimum and one maximum. We use $\beta_{\min}$ (or $\beta_{\max}$) to denote the value of β corresponding to the minimum (or the maximum). It is interesting that the value of β at which $-\alpha_i$ becomes maximum is nearly equal to $\beta_{\min}$. The existence of a maximum in the variation of the threshold value with β was unexpected; some remarks will be made about it later; except for this, our experiment verified the theoretical predictions. In fact, Ito's solution at $R = 5000$ agrees quite well with the experiment. Meksyn & Stuart (1951), Reynolds & Potter (1967) and Pekeris & Shkoller (1969) gave the threshold amplitude of disturbance stream function before Ito (1974*b*); these earlier results are not included in figure 16, owing to the lack of information required to estimate the threshold value of the u fluctuation; but the predictions of the earlier authors agree with the present experimental results qualitatively.

3.3.2. *Details of the subcritical growth process.* The growth process of a disturbance with $f = 72$ Hz at $R = 5000$, with initial intensity about 2%, was examined in detail to clarify the subcritical instability. Spectral analyses show that, as the fundamental grows, its higher harmonics develop in the streamwise

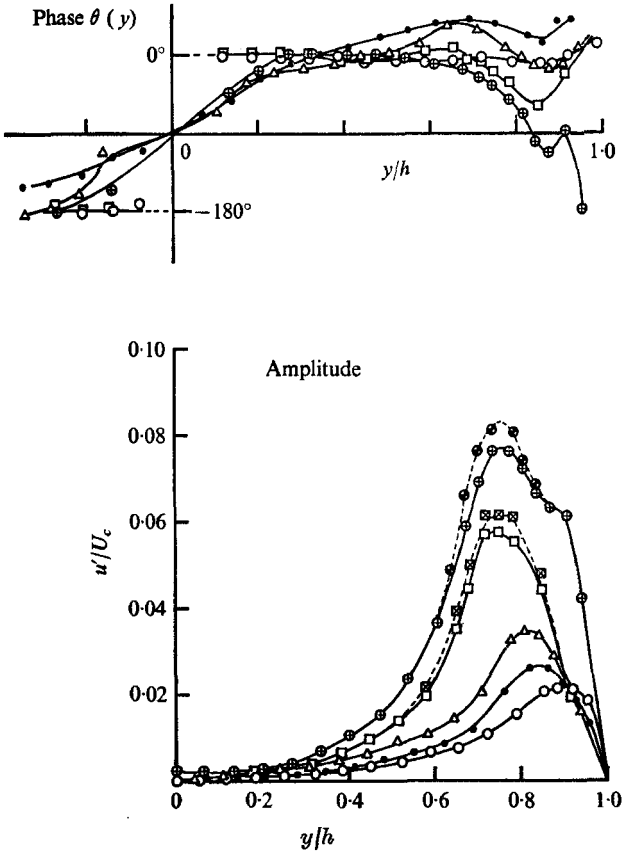

FIGURE 18. Changes in the amplitude and phase distributions of the fundamental fluctuation in the nonlinear subcritical growth of the disturbance illustrated by figure 17. ⊠, ⊕, total intensities.

Station	A	B	C	D		E	
	○	●	△	□	⊠	⊕	⊕

direction. This is illustrated in figure 17. The maximum r.m.s. values of the total and harmonic components are plotted on a logarithmic scale against $x-x_0$, which is expressed relative to $U_{c,0}$. The stations A–E in the figure are the streamwise positions where detailed observations were made. The subcritical instability sets in at about A. The initial growth of the fundamental is gradual; and the growth is rapid at C. The second harmonics start to grow at A, at a rate greater than that of the fundamental. This is evidence for the presence of nonlinear activity at an intensity of disturbance as low as 2 %. Downstream from station C, the third and fourth harmonics grow more rapidly than the fundamental and the second. No spectral components with frequencies smaller than the fundamental appear, until the line-like spectrum, centred at the fundamental 72 Hz, broadens appreciably downstream from C.

Whether a disturbance grows or damps must depend on amplitude and phase distributions and wavelength. Thus, it is interesting to see how the disturbance

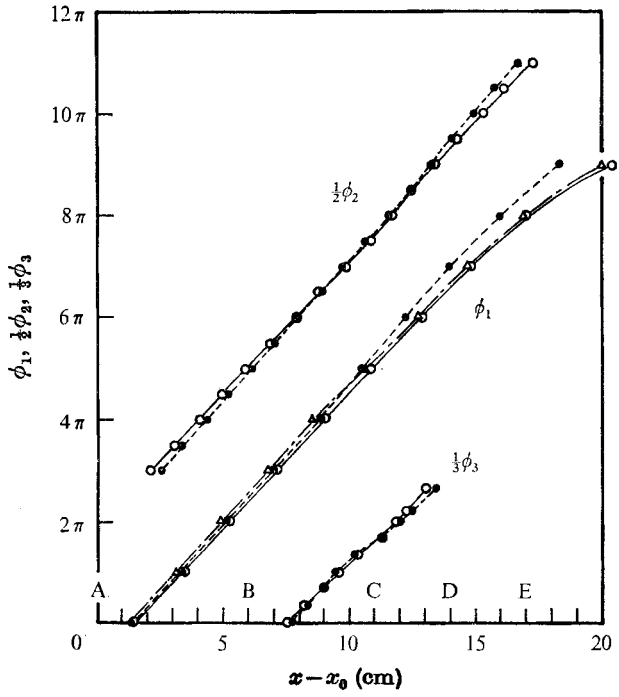

FIGURE 19. Streamwise variation of phase angles of harmonic components in nonlinear subcritical growth of the disturbance illustrated by figures 17 and 18. ϕ_1, ϕ_2, ϕ_3 represent the phase lags of the fundamental, second and third, respectively. Measurements made along lines y/h = const.

y/h	0·35	0·65	0·85
	△	○	●

under consideration changes during subcritical growth. The amplitude and phase distributions of the fundamental at stations A–E are given in figure 18. The distributions of the total r.m.s. value at D and E are also included in the figure. The distribution of the total is almost the same as that of the fundamental at each station. The distributions of the fundamental show the shapes predicted by linear theory at station A, but change downstream. The amplitude distribution changes in such a manner that the position of the maximum amplitude y_m moves towards the centre-plane $y = 0$; y_m/h varies from 0·88 at A to 0·75 at E. The phase distribution changes markedly. The 180° phase shift occurring around the centre-plane is almost discontinuous at A and D, but gradual at other stations. The amount of the shift occurring near the wall becomes larger downstream. Especially at E, a shift of more than 180° occurs between $y/h = 0{\cdot}5$ and 0·95. These features indicate that the fundamental changes its structure substantially during the growth process.

The streamwise variations of phases of harmonic components are shown in figure 19. In this figure ϕ_1, ϕ_2 and ϕ_3 denote the phase lags of the fundamental, second and third harmonics, respectively, all being expressed in radians. The phase relations between the three components are expressed arbitrarily. For ready comparison with the phase velocities, ϕ_1, $\frac{1}{2}\phi_2$ and $\frac{1}{3}\phi_3$ are plotted. These measurements were made along the lines $y/h = 0{\cdot}35$, 0·65 and 0·85. The variation of ϕ_1 along

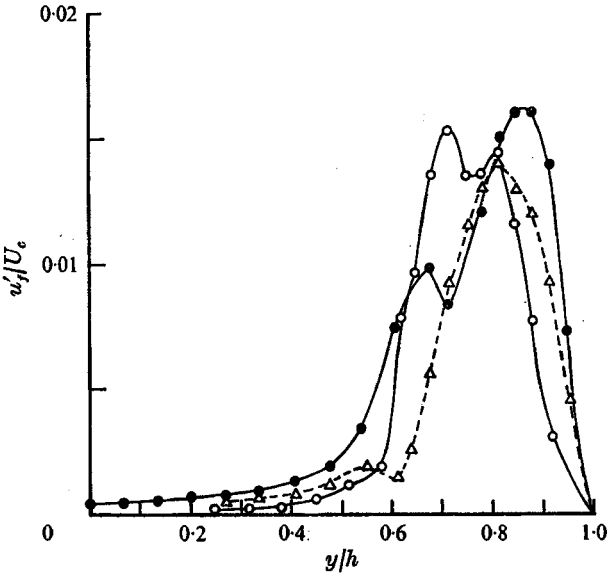

FIGURE 20. Amplitude distributions of higher-harmonic components in the nonlinear subcritical growth of the disturbance illustrated by figures 17–19. ○, second harmonic at station D; ●, the same at E; △, third at E.

these lines differs slightly, by amounts consistent with the phase distributions in the y direction in figure 18. Both $\frac{1}{2}\phi_2$ and $\frac{1}{3}\phi_3$ also show similar distributions. This suggests that the second and third harmonics change in structure downstream. The amplitude distributions of the second and third harmonics at D and E are given in figure 20. As for the fundamental, there is no significant departure of the phase velocity from that of the linear theory in the region up to D; $C = 0{\cdot}27U_c$ and $\lambda = 5{\cdot}2$ h (38 mm). But the phase velocity increases rapidly downstream from D. As can be seen from figure 19, the phase velocities of the second and third harmonics are equal to the phase velocity of the fundamental in the region up to C, but the three components travel at different phase velocities downstream from C.

The wave forms of the total u fluctuations at stations A–C are almost sinusoidal; those at D and E are largely distorted by the presence of higher harmonics of considerable magnitude. A notable feature is that, at E, an intense low-velocity pulse appears for each cycle of the fundamental at $y/h = 0{\cdot}8$ to $0{\cdot}9$. This is shown in figure 21 (plate 4). Instantaneous velocity distributions at E indicate that an inflexional velocity distribution with intense shear around $y/h = 0{\cdot}71$ appears when the pulse appears. As a result of the instability of the instantaneous distribution, the breakdown proceeds downstream just as happens in the case of the supercritical disturbance mentioned in § 3.2.

The mean velocity distributions are compared with the parabolic distribution in figure 22. Deviation from the parabolic distribution proceeds downstream, but it is small upstream of C. U_c remains almost constant upstream of E. In fact, even at E, $U_c = 0{\cdot}997U_{c,0}$. Hence, judging from figure 22, the flow rate across the half-depth is larger at station E than at stations A–D. This indicates that the

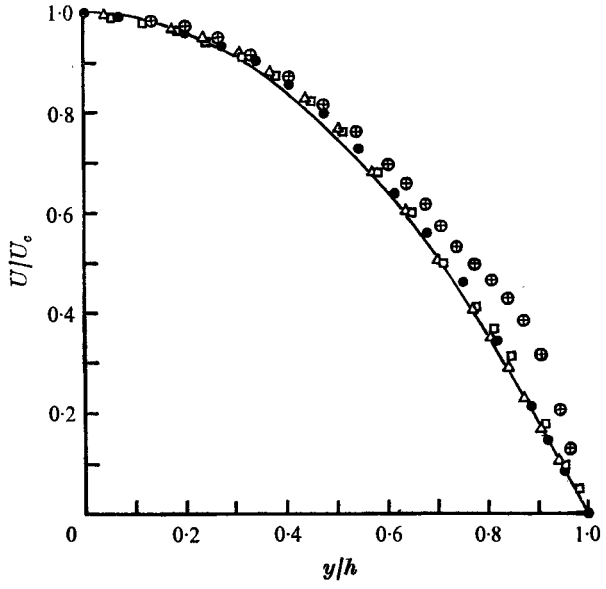

FIGURE 22. Mean velocity distributions in the nonlinear subcritical growth of the disturbance illustrated in figures 17–21. ——, parabolic distribution.

Station	B	C	D	E
	●	△	□	⊕

flow around E is three-dimensional. The reproducibility of the mean and fluctuation velocity fields mentioned so far is good upstream of E, but not so downstream from E. This suggests that the flow is three-dimensional there.

From similar observations at various values of R and f, it appears that the transition at subcritical Reynolds numbers proceeds as described above at $\beta \leqslant \beta_{\max}$ (mentioned in connexion with figure 16). It also appears that, at $\beta > \beta_{\max}$, the transition is triggered directly by spot-like fluctuations appearing abruptly before the fundamental has grown sufficiently. This is why the threshold value of u'_m/U_c decreases as β increases beyond $\beta_{\max}$ (see figure 16). We believe that this may be due to the highly three-dimensional nature of a disturbance with a large β. We should like to clarify our idea of the effect of the three-dimensionality on the subcritical instability; this must be done by controlling it as Klebanoff *et al.* (1962) did; the study is in progress.

4. Conclusion

In this paper we presented experimental results for the stability of a plane Poiseuille flow generated in a long rectangular channel with an aspect ratio of 27·4. The flow was maintained laminar up to $R = 8000$ by reducing the background turbulence down to a level of 0·05 %. The downstream development of the antisymmetric sinusoidal disturbance, which was introduced by means of a vibrating ribbon, was investigated in detail at $R = 3000$–7500. We compared the theoretical results of Ito (1947*a*, *b*), on linear and nonlinear stability, with our observations. We draw the following conclusions.

(i) The small disturbance behaves as predicted by linear stability theory.

(ii) Nonlinear subcritical instability occurs when the intensity of subcritical disturbances lies above a certain threshold value. The latter is found to be a function of Reynolds number and the frequency of disturbance. The experimental relations between the threshold value and the frequency obtained at $R = 4000$, 5000 and 6000 seem to support the theoretical relation of Ito (1974*b*).

(iii) The following are notable features observed in the initial stage of the subcritical growth process (i.e. in the region upstream of station C in figure 17). (*a*) The fundamental markedly changes its amplitude and phase distributions downstream. (*b*) The growth rates of the second and third harmonics are greater than that of the fundamental. (*c*) These harmonic components travel downstream at the same phase velocity. (*d*) The mean velocity distribution undergoes no large distortions.

(iv) Growth of the fundamental in both the subcritical and supercritical cases eventually leads to breakdown of the periodic motion and to transition to turbulence.

(v) As in the case of Blasius flow, breakdown occurs as a result of a local secondary instability of an inflexional velocity distribution, with intense shear appearing for each cycle of the fundamental oscillation.

The authors express their cordial thanks to Professor H. Sato, Institute of Space and Aeronautical Science, University of Tokyo, for suggesting this study, and for his helpful advice; and to Dr N. Ito, National Aerospace Laboratory, for kindly providing the results of his stability calculations.

REFERENCES

Badri Narayanan, M. A. & Narayana, T. 1967 *Z. angew. Math. Phys.* **18**, 642.
Davies, S. J. & White, C. M. 1928 *Proc. Roy. Soc.* A **119**, 92.
Ito, N. 1974*a* *Trans. Japan Soc. Aero. Space Sci.* **17**, 65.
Ito, N. 1974*b* *Trans. Japan Soc. Aero. Space Sci.* **17**, 160.
Kao, T. W. & Park, C. 1970 *J. Fluid Mech.* **43**, 145.
Karnitz, M. A., Potter, M. C. & Smith, M. C. 1974 *J. Fluids Engng*, **96**, 384.
Klebanoff, P. S., Tidstrom, K. D. & Sargent, L. M. 1962 *J. Fluid Mech.* **12**, 34.
Lin, C. C. 1955 *The Theory of Hydrodynamic Stability*. Cambridge University Press.
Meksyn, D. & Stuart, J. T. 1951 *Proc. Roy. Soc.* A **208**, 517.
Nishioka, M. & Sato, H. 1970 *Bull. ISAS, University of Tokyo*, **6**, 571. (In Japanese.)
Patel, V. C. & Head, M. R. 1969 *J. Fluid Mech.* **38**, 181.
Pekeris, C. L. & Shkoller, B. 1967 *J. Fluid Mech.* **29**, 31.
Pekeris, C. L. & Shkoller, B. 1969 *J. Fluid Mech.* **39**, 629.
Reynolds, W. C. & Potter, M. C. 1967 *J. Fluid Mech.* **27**, 465.
Schubauer, G. B. & Skramstad, H. K. 1943 *N.A.C.A. Rep.* no. 909.
Stuart, J. T. 1960 *J. Fluid Mech.* **9**, 353.
Stuart, J. T. 1971 *Ann. Rev. of Fluid Mech.* **3**, 347.
Thomas, L. H. 1953 *Phys. Rev.* **91**, 780.
Watson, J. 1960 *J. Fluid Mech.* **9**, 371.
Watson, J. 1962 *J. Fluid Mech.* **14**, 211.

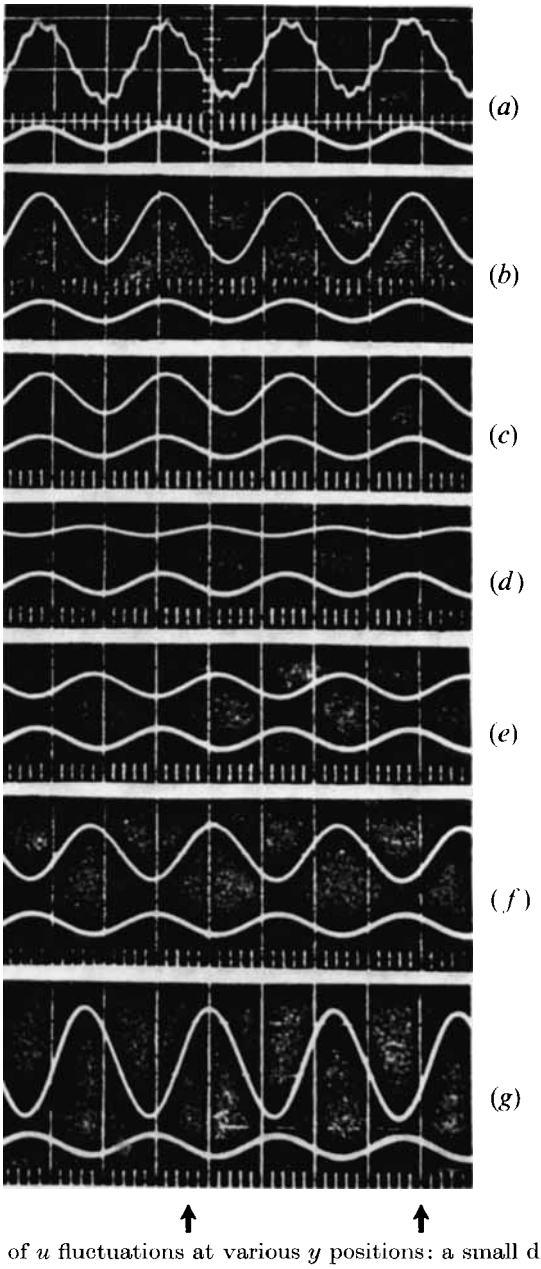

FIGURE 4. Wave forms of u fluctuations at various y positions: a small disturbance, with $f = 82$ Hz at $R = 6000$. Upper trace in (*a*)-(*g*) represents the u fluctuation, the lower the ribbon current.

	(*a*)	(*b*)	(*c*)	(*d*)	(*e*)	(*f*)	(*g*)
y/h	0·70	0·70	0·44	−0·01	−0·32	−0·60	−0·93

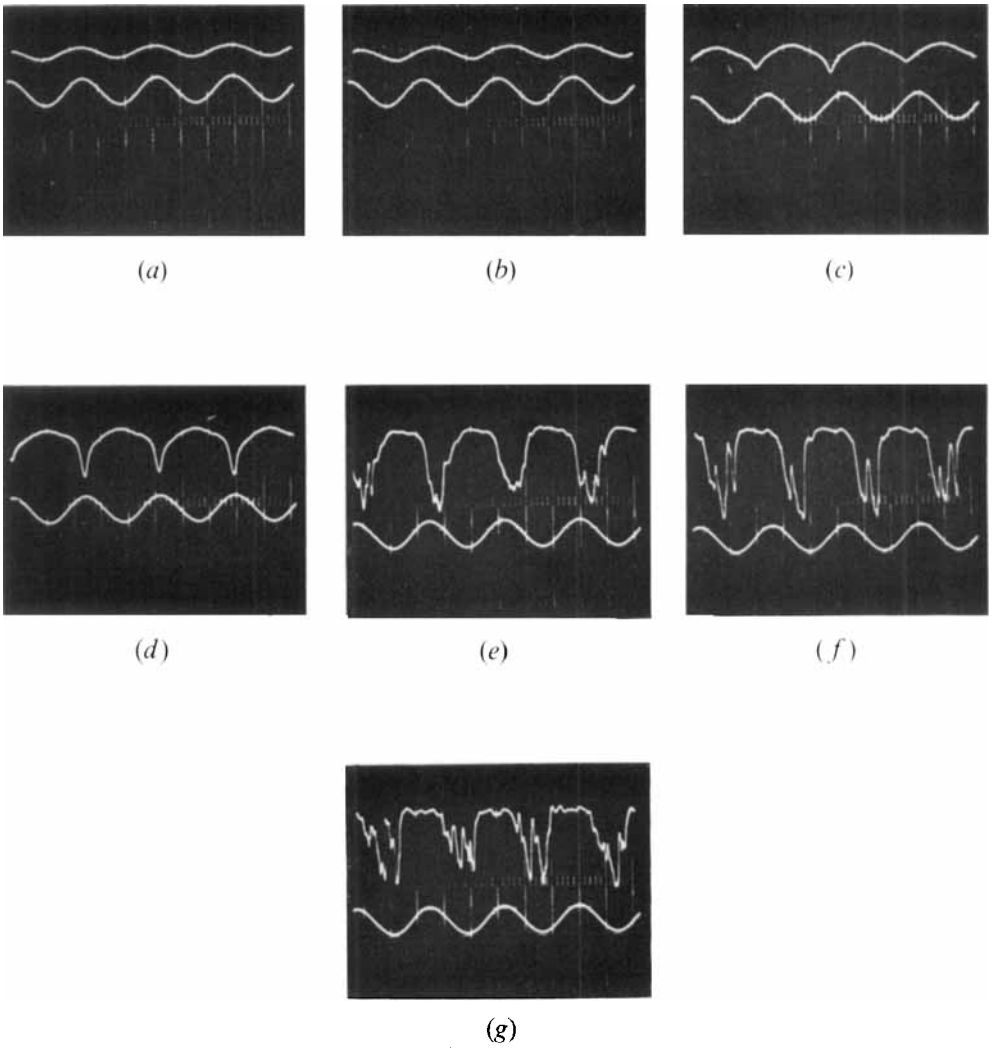

FIGURE 12. Appearance of low-velocity pulses and higher-frequency oscillations in the breakdown process of a supercritical disturbance, with a fundamental frequency $f = 72$ Hz at $R = 7200$. Upper trace in (*a*)–(*g*) shows the u fluctuation, the lower the ribbon current. Decreasing velocity in downward direction.

	(*a*)	(*b*)	(*c*)	(*d*)	(*e*)	(*f*)	(*g*)
$x - x_0$ (cm)	12	13	14	15	16	17	18
u'/U_c	0·018	0·025	0·058	0·102	0·131	0·131	0·109

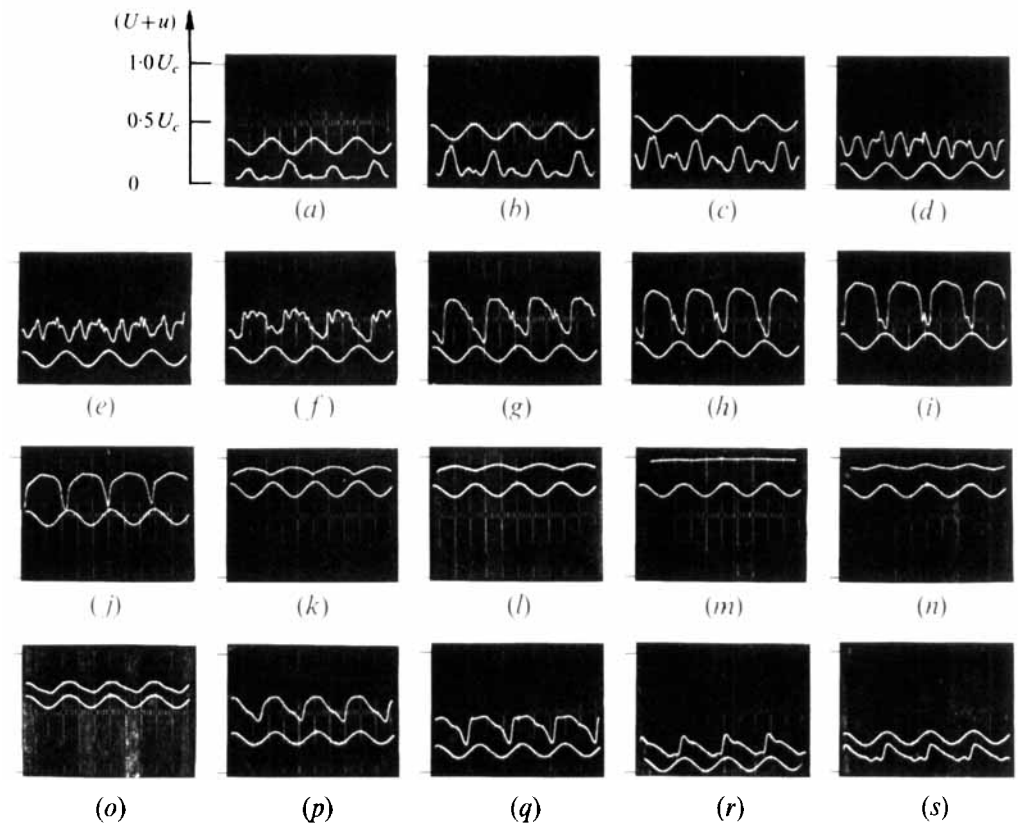

FIGURE 13. Wave forms of u fluctuations observed at various y positions, at $x-x_0 = 15$ cm, for the disturbance illustrated by figure 12. (*a*)–(*s*) indicate the instantaneous velocity $U+u$ and the ribbon current. y/h: (*a*) 0·97; (*b*) 0·96; (*c*) 0·93; (*d*) 0·86; (*e*) 0·80; (*f*) 0·73; (*g*) 0·66; (*h*) 0·60; (*i*) 0·53; (*j*) 0·47; (*k*) 0·40; (*l*) 0·30; (*m*) 0·02; (*n*) −0·23; (*o*) −0·49; (*p*) −0·62; (*q*) −0·76; (*r*) −0·89; (*s*) −0·92.

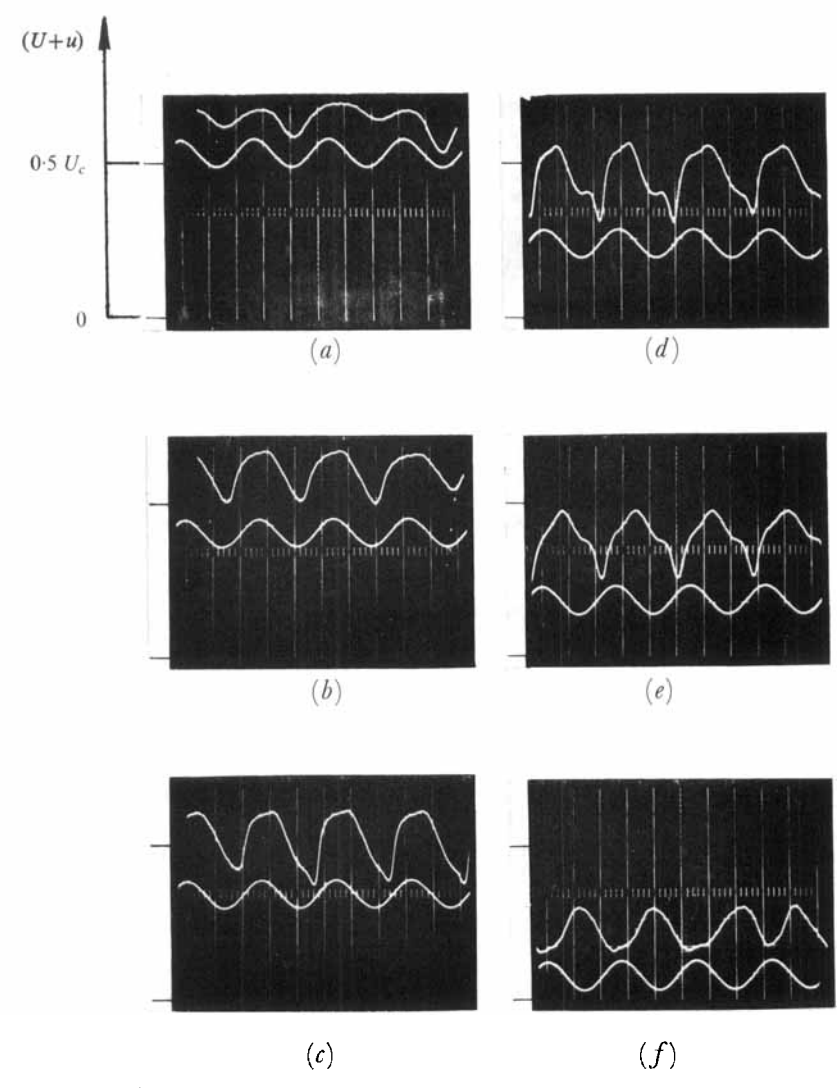

FIGURE 21. Wave forms of u fluctuations, at various y positions at station E, in the nonlinear subcritical growth of the disturbance illustrated by figures 17–20. (*a*)–(*f*) indicate the instantaneous velocity $U+u$ and the ribbon current.

	(*a*)	(*b*)	(*c*)	(*d*)	(*e*)	(*f*)
y/h	0·61	0·67	0·74	0·81	0·87	0·94